Energy Efficient Hybrid Silicon Electroabsorption Modulator for 40 Gb/s, 1-Volt Uncooled Operation

Yongbo Tang, Jonathan D. Peters, and John E. Bowers, *Fellow, IEEE*

***Abstract*—A high speed and energy-efficient lumped electroabsorption modulator has been demonstrated on the hybrid silicon platform for uncooled operation up to 80°C. This 100 μm long modulator has a 3 dB bandwidth of around 30 GHz. Eye diagrams measured at the temperatures of 20°C, 40°C, 60°C and 80°C with corresponding adjustment on the input wavelength and the bias voltage show a dynamic extinction ratio of around 5 dB at 40 Gb/s with a 1 V drive voltage swing and an energy consumption of ~112 fJ/bit.**

***Index Terms*—Waveguide modulator, electroabsorption, integrated optics, silicon-on-insulator (SOI).**

I. Introduction

THE need for fast and energy-efficient communications is driving optical interconnects for short and long reach applications, due to its wide bandwidth, large capacity, long transmission distance, low latency, and immunity to electromagnetic interference. Silicon-based optical interconnect solutions are desired for a short transmission distance for board- or even chip-level interconnects due to the low cost and quality control of CMOS foundries for the production of silicon photonic integrated circuits (PICs) and also due to the ease of integration using a common material system for both electronic integrated circuits and PICs.

An energy consumption of 1 pJ/bit is an important technical milestone for optical solutions to be more attractive than electrical interconnects for short distance interconnects [1]. For lasers, this means low threshold and high efficiency. For modulators, this target drives lower loss, higher speed and reduced drive voltage. The energy per bit can be directly scaled if the speed is upgraded to a higher transmission rate. Reducing the drive voltage means less energy consumption from the modulators. More importantly, if it can be less than 1 V, the logical output of advanced CMOS drivers can be directly applied to the modulator, leading to a much simpler circuit and lower energy consumption. Additionally, for applications in a high temperature environment, it is very important to realize uncooled operation to avoid the use of the thermoelectric (Peltier) coolers, which currently dominate energy consumption inside optical transmitter [2].

1-volt operation at 25 Gb/s has been demonstrated on silicon microring modulators [3] and Mach-Zehnder modulators [4]. However, the use of the high-Q resonator for the ring modulator makes it very sensitive to temperature and fabrication perturbations, typically requiring additional heaters and feedback loops for tuning and stabilization. Since the silicon Mach-Zehnder modulators rely on a low impedance terminator (usually no greater than 50 Ω) to realize the traveling-wave configuration for high speed operations, they are usually less attractive for low energy consumption compared with those without terminators.

Unlike silicon, III-V materials are good for optical modulation and have been demonstrated for commercial products with advantages of large optical and electrical bandwidth, low drive voltage, compact size, as well as integration compatibility with semiconductor lasers. We have shown that a high quality III-V layer stack can be transferred onto the silicon substrate using the wafer bonding technique [5]. Hybrid silicon electroabsorption modulators (HSEAM) with distributed electrodes have been developed for applications beyond 50 Gb/s [6], [7]. However, to achieve very low energy consumption, lumped modulators with high input impedances are preferable. Previously, Y. Kuo et al. have demonstrated a lumped hybrid silicon electroabsorption modulator with a sub-volt drive voltage swing for 10 Gb/s operation [8]. In this paper, we will show that with a better design and an improved process the bandwidth of the lumped hybrid silicon modulator can be increased to around 30 GHz and 1-volt operation at 40 Gb/s is demonstrated for uncooled operation up to 80°C with corresponding adjustment on the input wavelength and reverse bias.

II. Structure and Fabrication

Fig. 1(a) shows the schematic structure of this hybrid silicon electroabsorption modulator. The lumped electrode configuration gives a very compact design with a footprint of 150 μm $\times$ 250 μm, limited primarily by the probe pads that are used here for testing (see Fig. 1(b)). The size can be further reduced if the device is connected to the driving circuits through metal interconnects [9] or microsolder bumps by flip-chip bonding [10]. This device consists of a 100 μm long effective modulation segment and two 70 μm multiple-level adiabatic tapers. The cross section of the modulator segment can be found in the photo of Fig. 1(c), which is shot under a tilt angle of 52°. It is composed of a silicon ridge and a III-V p-i-n structure. The silicon ridge was defined on a 400 nm thick silicon layer by using a 200 nm-depth dry etch. The III-V structure above the silicon ridge includes a 4 μm wide, 1.5 μm high gradually-doped (2e18 to 1e18 cm^{-3}) p-InP mesa, a 1.85 μm wide intrinsic layer, and a thin n-InP

The authors are with the Department of Electrical and Computer Engineering, University of California Santa Barbara, Santa Barbara, CA 93106, USA. (E-mail: ytang@ece.ucsb.edu, peters@ece.ucsb.edu, bowers@ece.ucsb.edu).

Manuscript received on June 15, 2012.

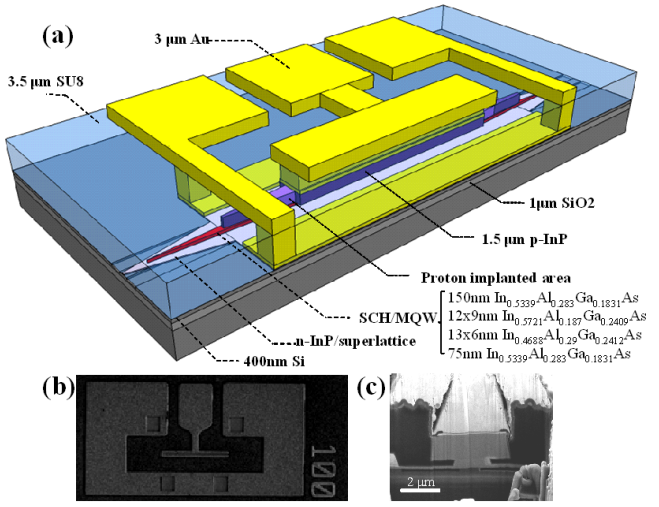

Fig. 1. Schematic diagram, and SEMs of the lumped hybrid silicon EAM.

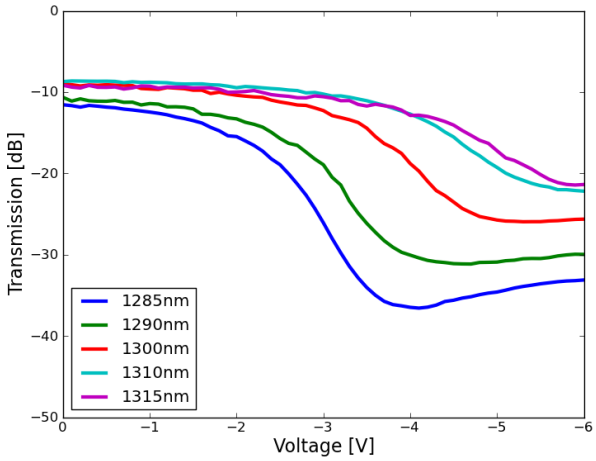

Fig. 2. Bias-dependent transmission at 20°C for a 30 nm wavelength range.

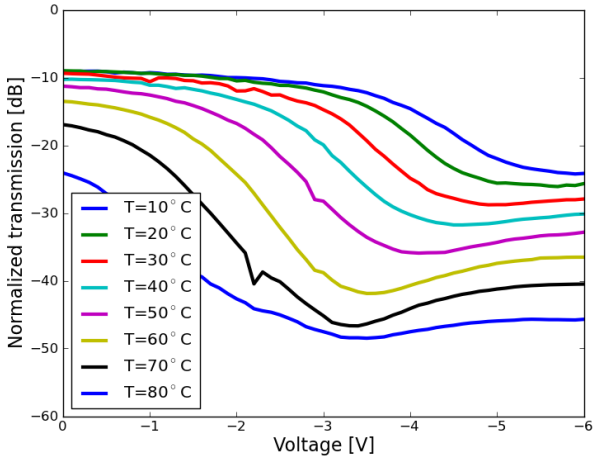

Fig. 3. Bias-dependent transmission at 1300 nm within the temperature range of 10°C to 80°C.

extending to the lateral ground metal. The detailed structure of the intrinsic region including the SCH and the MQW is shown in Fig. 1(a) and more information about the epitaxial layers can be found in [7]. The width of the intrinsic region was reduced by an undercut operation through selective wet etching. The undercut process is monitored under a microscope and the control of the etch depth is based on a reference pattern with the target marked on the silicon layer underneath. The transition tapers between the silicon waveguide and the modulation segment are realized on four different material layers. As shown in Fig. 1(a), three levels of the taper are defined on the n-InP, MQW/SCH and the p-Mesa, respectively. They are shrunk one layer by one layer with the upper taper tip moving closer to the modulation segment, forming a quasi-vertical taper structure. The taper tips of the n-InP and the p-Mesa are around 400 nm, limited by resolution of the I-line lithography; while the tip width of the MQW/SCH was reduced to less than 100 nm through the wet etching step. The fourth-level taper is defined on the silicon waveguide (not visible in Fig. 1(a)), with the ridge width reduced from 2 μm to 1 μm towards the modulation segment. In order to reduce the device capacitance for high speed operation, the tapers have to be electrically isolated from the main part of the modulator. This is achieved by applying proton implantation to the p-mesa. The 10 μm long implantation area is located at the end of the taper as shown in Fig. 1(a).

III. CHARACTERIZATION

We initially characterized the modulator's static transmission performance as a function of the reverse bias at 20 °C. The measured data for input wavelengths from 1285 nm to 1315 nm are shown in Fig. 2. The data is normalized by the insertion loss of the reference blank silicon waveguides. We can see that this modulator can support a wavelength window of 30 nm with an extinction ratio larger than 10 dB for a 2 V bias change although the insertion loss is increased from ˜9 dB to 11.5 dB towards a shorter wavelength due to the increased residual absorption. This insertion loss is higher than expected. Misalignment between the MQW layer and the silicon waveguide (an offset of ˜160 nm is found from the cross-section), the rough sidewall of the intrinsic region due to the nonuniform undercut rate for different compositions and unexpected residues attached to the tapers might be the primary reasons behind this. We then fixed the input wavelength at 1300 nm and measured the static transmission under different temperatures. As shown in Fig. 3, a high temperature leads to a similar curve as the case in Fig. 2 for a shorter wavelength. This is due to the temperature-induced red shift of the absorption spectrum. Up to 50°C, the penalty of the insertion loss is less than 2 dB. Based on the comparison of Fig. 2 and Fig. 3, we estimate that the red shift rate is slightly larger than 0.5 nm/°C, which matches the typical shift rate of the gain peak for a semiconductor optical amplifier [11].

In the following measurements at different temperatures, the input wavelength is correspondingly tuned at a rate of 0.5 nm/°C. Fig. 4 shows the measured small-signal modulation responses. For the temperature range from 20°C to 80°C, the

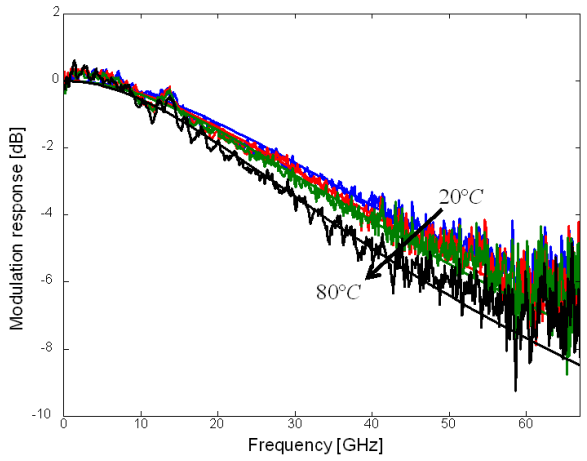

Fig. 4. Measured modulation responses at different temperatures.

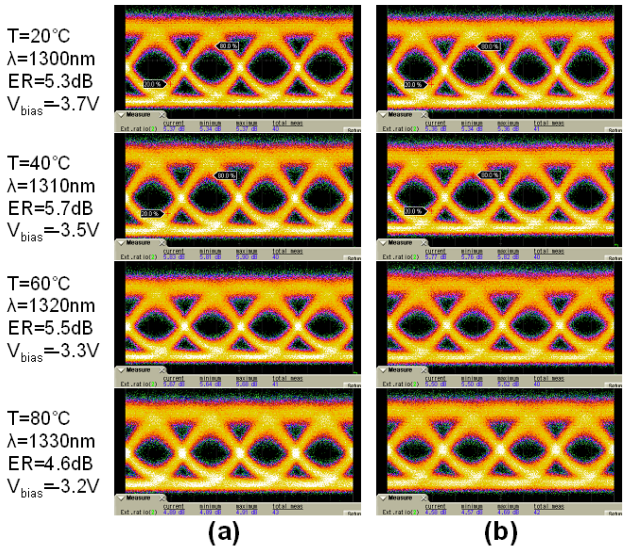

Fig. 5. Measured eye diagrams at 40 Gb/s with a 1 V drive voltage for (a) back-to-back transmissions and (b) the transmissions through a 10.9 km single mode fiber at different temperatures.

3 dB electro/optical bandwidth is maintained around 30 GHz, although a weak degradation is observed as the temperature increases. One reason for the degradation is the increase of the series resistance since the carrier mobility in the doped InP drops at a higher temperature [12].

Large signal measurements were carried out at 40 Gb/s. The 2^31-1 PRBS signal was amplified and then went through a 23 dB RF attenuator and a bias tee to get an appropriate drive voltage. The electric eye diagram captured by a DCA with a 50 Ω input impedance shows an eye amplitude of 494 mV. Since a lumped HSEAM can be treated as an open terminator where the reflection is constructively added to the forward voltage at the end, this configuration gives a total drive voltage swing of around 1 V applied to the modulator.

In order to compensate the fiber to chip coupling loss, a semiconductor optical amplifier and a 1 nm tunable filter are added after the modulator. For the back-to-back measurement, the optical receiver is connected just after the filter. We also demonstrated the case with a 10.9 km single mode fiber inserted between the tunable filter and the optical receiver to explore the long distance transmission performance. All of the measurements are operated with the same input optical power of ~5 dBm and the bias voltage as listed in Fig. 5 is adjusted to get a ~ 1 mA averaged bias current. The on-state loss is estimated to be 12-13 dB. Fig. 5 shows the measured eye diagrams at 40 Gb/s at the temperatures of 20°C, 40°C, 60°C and 80°C for the two cases. These eyes are open and present a dynamic extinction ratio of around 5 dB.

The energy consumption of this hybrid silicon modulator can be calculated by

$$E = CV_{\mathrm{pp}}^2/4 + I_{\mathrm{average}}V_{\mathrm{bias}}/B \quad (1)$$

The first item represents the transient energy consumption for the capacitor charging, where C is the junction capacitance and V_{pp} is the peak to peak drive voltage; the second item denotes the DC energy consumption, where V_{bias} is the bias voltage, I_{average} is the averaged DC current (mainly contributed by the photocurrent) and B is the transmission bit rate. The capacitance of this modulator is around 80 fF and it gives a transient energy consumption of 20 fJ/bit for this 1-volt operation. To get similar transient energy consumption, a distributed modulator with a matched 50 Ω input impedance has to be operated at a voltage swing of 0.4 V, according to the formula given in [7]. The DC energy consumption at 40 Gb/s is 92.5 fJ/bit. This DC consumption can be down-scaled with a reduced input optical power. A more essential way to cut it down relies on the reduction of the bias voltage, which may be achieved by optimizing the quantum well with the photoluminescence peak shifted closer to the working wavelength and at the same time maintaining the insertion loss at an acceptable level.

IV. Conclusion

In summary, 1-volt uncooled operation at 40 Gb/s has been demonstrated on a hybrid silicon modulator with a lumped configuration. 5 dB dynamic extinction ratios have been obtained for both the back-to-back transmissions and the transmissions through a 10.9 km single mode fiber at the temperatures of 20°C, 40°C, 60°C and 80°C with optimized input wavelength and reverse bias, respectively. The total energy consumption of the hybrid silicon modulator for this measurement is around 112.5 fJ/bit including the contribution from the photocurrent.

Acknowledgment

This work was supported by the DARPA MTO EPHI program. The authors thank Scott Rodgers, Urban Westergren, Daoxin Dai, Doug Baney, Hui-Wen Chen, Siddharth Jain, Daryl Spencer, Ling Liao and Matthew N. Sysak for useful discussions.

REFERENCES

[1] A. V. Krishnamoorthy, K. W. Goossen, W. Jan, X. Zheng, R. Ho, G. Li, R. Rozier, F. Liu, D. Patil, J. Lexau, H. Schwetman, D. Feng, M. Asghari, T. Pinguet, and J. E. Cunningham, "Progress in Low-Power Switched Optical Interconnects," *IEEE Journal of Selected Topics in Quantum Electronics*, vol. 17, no. 2, pp. 357-376, Apr. 2011.

[2] W. Kobayashi, M. Arai, T. Yamanaka, N. Fujiwara, T. Fujisawa, T. Tadokoro, K. Tsuzuki, Y. Kondo, and F. Kano, Design and Fabrication of 10-/40-Gb/s, Uncooled Electroabsorption Modulator Integrated DFB Laser With Butt-Joint Structure, *J. Lightwave Technol.*, vol. 28, no. 1, pp. 164-171, Jan. 2010.

[3] G. Li, X. Zheng, J. Yao, H. Thacker, I. Shubin, Y. Luo, K. Raj, J. E. Cunningham, and A. V. Krishnamoorthy, "25Gb/s 1V-driving CMOS ring modulator with integrated thermal tuning," *Opt. Express*, vol. 19, no. 21, pp. 20435-20443, Oct. 2011.

[4] T. Baehr-Jones, R. Ding, A. Ayazi, T. Pinguet, M. Streshinsky, N. Harris, J. Li, L. He, M. Gould, Y. Zhang, A. E.-J. Lim, T.-Y. Liow, S. H.-G. Teo, G.-Q. Lo, and M. Hochberg, "A 25 Gb/s Silicon Photonics Platform," arXiv:1203.0767, Mar. 2012.

[5] D. Liang, G. Roelkens, R. Baets, and J. E. Bowers, "Hybrid integrated platforms for silicon photonics," *Materials*, vol. 3, no. 3, pp. 1782-1802, 2010.

[6] Y. Tang, H.-W. Chen, S. Jain, J. D. Peters, U. Westergren, and J. E. Bowers, "50 Gb/s hybrid silicon traveling-wave electroabsorption modulator," *Opt. Express*, vol. 19, no. 7, pp. 5811-5816, Mar. 2011.

[7] Y. Tang, J. D. Peters, and J. E. Bowers, "Over 67 GHz bandwidth hybrid silicon electroabsorption modulator with asymmetric segmented electrode for 1.3μm transmission," *Opt. Express*, vol. 20, no. 10, pp. 11529-11535, May 2012.

[8] Y. Kuo, H. Chen, and J. Bowers, "High speed hybrid silicon evanescent electroabsorption modulator," *Opt. Express*, vol. 16, pp. 9936-9941, 2008.

[9] A. Uddin, K. Milaninia, C.-H. Chen, and L. Theogarajan, "Wafer Scale Integration of CMOS Chips for Biomedical Applications via Self-Aligned Masking," *IEEE Transactions on Components, Packaging and Manufacturing Technology*, vol. 1, no. 12, pp. 1996-2004, Dec. 2011.

[10] X. Zheng, F. Y. Liu, J. Lexau, D. Patil, G. Li, Y. Luo, H. D. Thacker, I. Shubin, J. Yao, K. Raj, R. Ho, J. E. Cunningham, and A. V. Krishnamoorthy, "Ultralow Power 80 Gb/s Arrayed CMOS Silicon Photonic Transceivers for WDM Optical Links," *J. Lightwave Technol.*, vol. 30, no. 4, pp. 641-650, Feb. 2012.

[11] L. A. Coldren and S. W. Corzine, *Diode Lasers and Photonic Integrated Circuits*, 1st ed. Wiley-Interscience, 1995.

[12] V. V. Galavanov and N. V. Siukaev, "On Mechanism of Electron Scattering in InP," *physica status solidi (b)*, vol. 38, no. 2, pp. 523-530, 1970.